



ATLAS Jet Energy Scale Uncertainty: An analysis of the Jet Energy Resolution using random cones

Advisors: Prof. M. Oreglia, K. Hildebrand

Kevin Ullmann

ATLAS Jet Energy Scale Uncertainty: An analysis of the Jet Energy Resolution using random cones

K. Ullmann

May 27, 2017

Abstract

Hadronic jets are an important object of study in the ATLAS experiment at the LHC at CERN. Jets are characterized by an energy-momentum four-vector, so a precise measurement of jet energy is vital to collision analysis. These jet energies are calibrated in a multi-step process to bring them to the jet energy scale (JES). The uncertainty in the jet energy scale is characterized by the jet energy resolution. This article describes the JES calibration procedure, and presents an analysis of the calibration using the random cones method to measure one key component of the jet energy resolution, the noise term.

1 Introduction

1.1 Aims of this article

The ATLAS experiment employs a complicated calibration process for the analysis of pp collision energies. The goal of this paper is to measure one component of the jet energy uncertainty - the noise term - using the so-called random cones method. We will demonstrate how the random cones method is used to further understand the jet energy resolution (JER) by calculating the noise term at the JES.

The article proceeds in seven sections. In section 1, an overview of ATLAS is given and the jet energy scale and jet energy resolution are explained. In section 2 we discuss sources of errors and uncertainties that comprise the jet energy resolution. Section 3 goes into some detail about the JES calibration process commonly used by ATLAS; this is the process to be analyzed by the random cones method. In section 4 the random cones method itself is discussed. Finally, results about the characterization of the JER are presented in section 5, with a summary of conclusions in Section 6. For additional technical details on how this study was carried out, see the appendix (A).

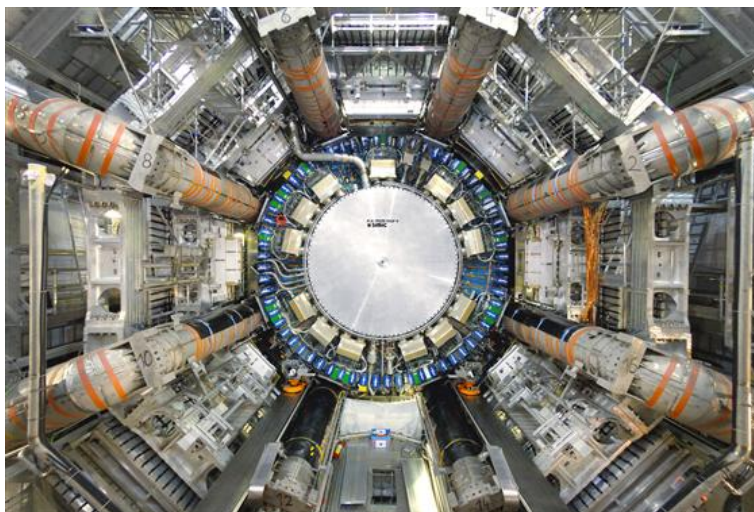


Figure 1: The ATLAS detector, under construction (missing central detector)
ATLAS Experiment ©2007 CERN

1.2 Description of ATLAS instruments

The ATLAS experiment features a multi-purpose detector designed to observe individual particles and particle jets produced in the proton-proton collisions at the LHC. The main components of the ATLAS detector are, from center outward, the inner tracking detector (ID), electromagnetic and hadronic sampling calorimeters, and the muon spectrometer (MS). [2]

The ID has complete azimuthal coverage, and spans the pseudorapidity region $|\eta| < 2.5$ [2]. This component consists of layers of silicon pixel, silicon microstrip and transition radiation tracking detectors. These sub-detectors are surrounded by a superconducting solenoid that produces a uniform 2 T axial magnetic field. This detector is used to reconstruct tracks from charged particles and determine their transverse momenta from the curvature of the tracks. [7]

Jets are reconstructed from energy deposited in the ATLAS calorimeter system. Electromagnetic calorimetry is provided by high granularity liquid argon (LAr) sampling calorimeters, which are split into barrel ($|\eta| < 1.475$) and endcap ($1.375 < |\eta| < 3.2$) regions. In addition, inside this layer of calorimeters, a LAr based presampler layer is included which allows corrections for energy loss due to showers initiated by material before the calorimeters. Lead plates are used for absorption and span the entire η region. [4]

The hadronic calorimeter is divided into the barrel ($|\eta| < 0.8$) and two extended barrel ($0.8 < |\eta| < 1.7$) regions, which are instrumented with scintillator tile/steel calorimeters and the hadronic endcap region ($1.5 < |\eta| < 3.2$), which uses LAr/copper calorimeter modules. The forward calorimeter region ($3.1 < |\eta| < 4.9$) is instrumented with LAr/copper and LAr/tungsten modules to provide electromagnetic and hadronic energy measurements, respectively. The electromagnetic and hadronic calorimeters are segmented in layers, allowing a determination of the longitudinal profiles of showers. [4]

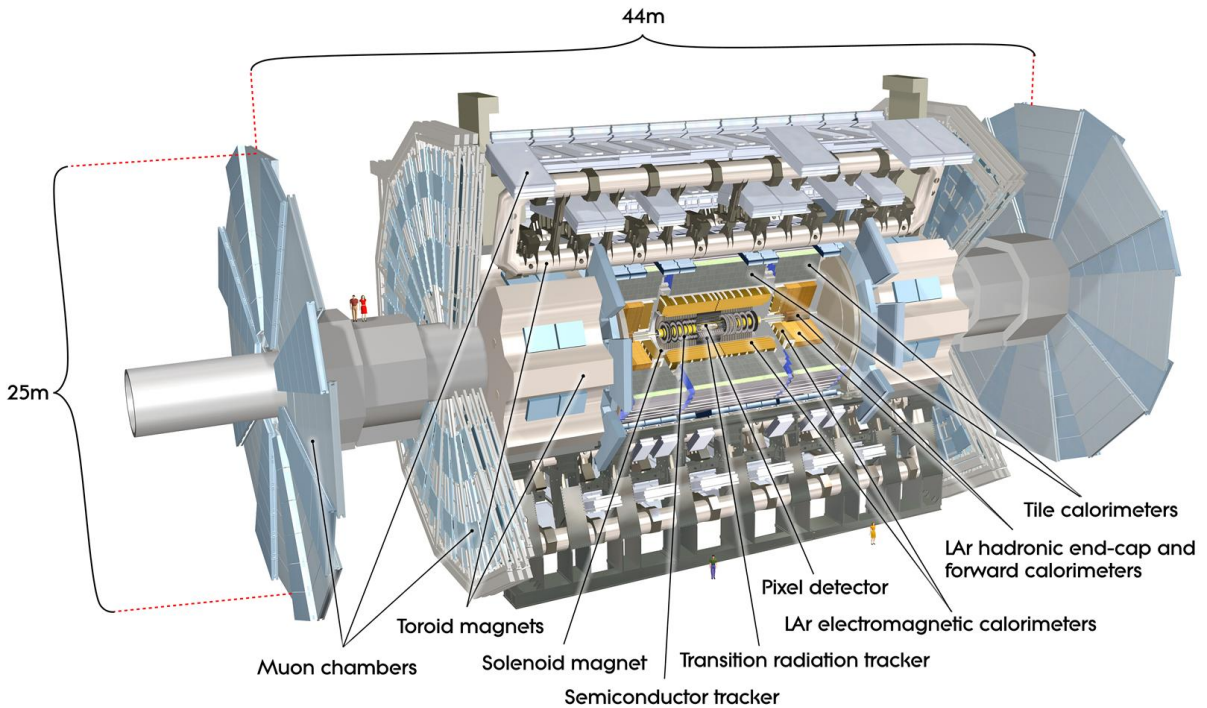


Figure 2: Schematic rendering of the ATLAS detector
 ATLAS Experiment ©2016 CERN

An ATLAS trigger system filters events to be stored. The trigger system consists of a hardware-based trigger (L1) followed by a software-based higher level trigger (HLT) [3]. Jets are first identified at L1 using a sliding window algorithm using coarse granularity calorimeter towers as input. This data is refined using jets reconstructed from calorimeter cells in the HLT.

1.3 Definitions: Jets, JES, and JER

Jets are the dominant final state objects of high-energy pp interactions at the LHC. They are collimated streams of particles that result after the collisions occur, when a quark or gluon decays and creates a cascade, or shower, of additional quarks and gluons.

Jets are detected using data from all components of ATLAS. The inner detector measures tracks of charged particles. When these particles decay, they produce a shower of partons, which then deposit their energy in the calorimeters. The energy is deposited in topologically related clusters, and these clusters comprise the jets. Various algorithms, for example the commonly used anti-kt algorithm [11], are employed to determine jets from the clusters. These jets can usually be associated with the tracks from the ID. The jets are calibrated using the multi-step process described in section 3.

When jets are constructed from collision data, they begin at an energy scale known as the "constituent scale." There are two separate constituent scales, which are both used to reconstruct jets from the same datasets. These are the EM scale, which reconstructs jets from data assuming the constituents are, e.g. electrons, and the local cluster weighting (LCW) scale, which reconstructs jets assuming the constituents are hadrons. The calibration brings the jets from the constituent scale to the JES in a series of steps. [10]

Three separate corrections are made to the constituent scale jets: origin correction, and in-time and out-of-time pileup correction. These steps are described in more detail below. These corrected constituent scale jets are then further corrected to match "truth jets" from Monte Carlo simulations. Truth jets are reconstructed using the same algorithm as calorimeter jets, but using truth particles with a lifetime greater than 30 ps as input, excluding muons and neutrinos. Only calorimeter and truth jets with $p_T > 7$ GeV and $|\eta| < 4.5$ are used. [10]

The Monte Carlo (MC) corrections are designed such that the jet response, which is the ratio of calorimeter jet p_T to truth jet p_T (reconstructed using the same algorithm), is equal to unity. After this step in the calibration process, the jets are said to be at the jet energy scale.

The jet energy resolution (JER) is the uncertainty in the final measurement of the jet energy after all calibration is completed. It is computed by comparing measurements to simulation. Further refinements to the jets are made at the JES, including global sequential calibration and residual in-situ calibration, which improve the resolution without affecting the average jet p_T . [1]

2 Sources of Errors and Uncertainties in Measurement

Calibration to the JES is necessary due to the multiple sources of noise and uncertainty when taking measurements from ATLAS. Some of the main effects that require corrections include: [10]

1. **Calorimeter non-compensation:** Corrections are necessary to account for the two different constituent scales. It is not known a priori what kind of particle produced a given measurement, and the calorimeter has a different energy response to EM interactions versus hadrons, so a measurement of the energy must take this difference into account.
2. **Dead material:** Energy lost in inactive areas of the detector
3. **Electronic noise:** Fluctuations in signal, an unavoidable characteristic of all electronic circuits
4. **Leakage:** Showers which reach the outer edges of the detector will not deposit all of their energy in the calorimeters
5. **Missing particles:** The energy of particles which are included in the truth jet but were not included in the algorithmically reconstructed jet
6. **Energy deposits below noise thresholds:** Only energy deposits above background noise are included in the clusters used to reconstruct jets. Some particles may not pass this threshold and these must be accounted for.
7. **Pile-up (in-time):** Multiple pp interactions may occur in the same bunch crossing
8. **Pile-up (out-of-time):** Residual signals from other bunch crossings may also affect energy readings

In recent years, pile-up has become increasingly significant, due to the operation of the LHC at higher energies and intensity (luminosity). The mean number of inelastic pp interactions per bunch crossing, $\langle\mu\rangle$, is related to the instantaneous luminosity, L : [6]

$$\langle\mu\rangle = \frac{L \times \sigma_{inel}}{N_{bunch} \times f_{LHC}}$$

where σ_{inel} is the total inelastic pp cross-section and $N_{bunch} \times f_{LHC}$ is the average frequency of bunch crossings in the LHC. The instantaneous luminosity in 2012 reached values as high as $7.7 \times 10^{33} \text{ cm}^{-2} \text{ s}^{-1}$, and the average pile-up activity in 2012 was $\langle\mu\rangle \approx 20.7$ interactions per bunch crossing. In-time-pileup, which is the presence of additional interactions in the same bunch crossing as the triggered event, produced additional signals in the ATLAS calorimeters, while the LHC bunch spacing of 50 ns allowed for out-of-time pileup: further signal modulation from multiple interactions in surrounding bunch crossings. [6]

3 JES Calibration

Now we will describe in detail the main calibration procedure that was analyzed in this study. The following procedure takes the jets from the constituent scale to the JES, and applies a few final corrections. The entire procedure is summarized in figure 3. This section will describe each step of the process.

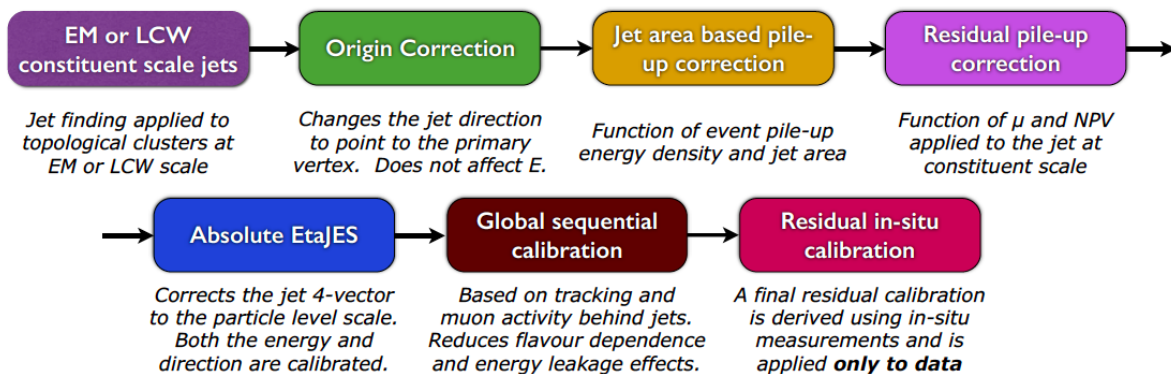


Figure 3: Calibration process (Source: Ref [10])

3.1 Origin Correction

The ATLAS calorimeters measure the energy of particles. A direction is needed to specify the full 4-vector of the jet. A simple choice is to point the vectors at the center of the detector, however, the position of the first primary vertex (determined by the highest p_T tracks) proves to be a better choice after full reconstruction of the event. Origin correction thus consists of finding the energy center of the jet and modifying the jet 4-vector such that the energy is unchanged but the direction originates from the first primary vertex, which is defined by that vertex having the highest $\sum p_T^2$ of tracks (with $p_T > 400$ MeV) associated with it. [10]

Figure 4 shows an example event recorded by ATLAS. The first primary vertex is at the center, the blue cones, which are jets, are pointing back at it. On the left there is a zoomed out view of a two tau event. The taus decay into an electron (blue line) and a muon (red line). On the right is a close up view of an event with four primary vertices, shown in the center in red.

3.2 Pile-up Correction

Pile-up noise is removed using an area based subtraction method. [10] This removes the effect of pile-up by using the pile-up energy density in the $\eta \times \phi$ plane ¹

¹Ref [10] explains these coordinates: "The ATLAS coordinate system is right-handed, with the x -axis pointing to the centre of the LHC ring, the z -axis following the beam direction and the y -axis pointing upwards. The azimuthal angle

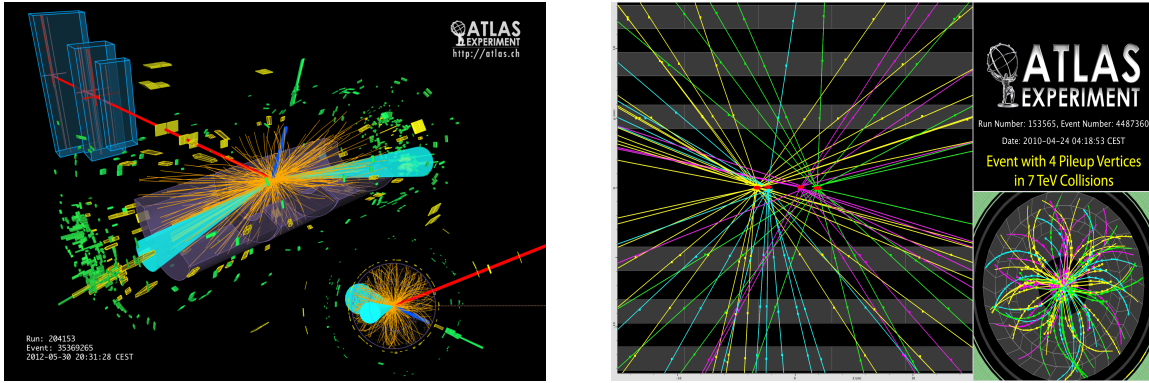


Figure 4: ATLAS events

Observations reveal that after this correction is applied a small dependence of the jet p_T on pile-up remains, so an additional residual correction is needed. This correction is parameterized by the number of primary vertices, NPV , and the average number of interactions per bunch crossing, $\langle\mu\rangle$, so that both the residual in-time, characterized by NPV (at fixed η), and out-of-time, characterized by η (at fixed NPV), pile-up dependence can be captured.

The pile-up subtracted p_T , following area based correction and residual correction, p_T^{corr} , is therefore given by:

$$p_T^{\text{corr}} = p_T^{\text{const}} - \rho \times A - \alpha \times (NPV - 1) - \beta \times \langle\mu\rangle$$

where α and β are jet size and algorithm dependent constants derived from Monte Carlo and p_T^{const} is the jet p_T at the topo-cluster scale. [6]

3.3 Jet Energy Scale

At this point another correction is applied, after which the data is said to be at the "jet energy scale." The jet energy scale calibration is derived from relating the reconstructed jet energy to the truth jet energy [5]. The JES factors are derived from isolated jets from an inclusive jet Monte Carlo sample after the pile-up and origin corrections have been applied. Following the calibration in energy it is found that in particular regions of the detector there is a bias in the η distribution with respect to the truth jets. Therefore, an additional correction to the angle of the jet is applied to resolve this bias. This also improves the closure in p_T of jets, where the closure in a given quantity is defined by the fit of a Gaussian function to the reconstructed quantity divided by the truth quantity after calibration.

3.4 Global Sequential Correction

After correcting to the JES, there is a difference between the closure - the deviation from unity of the jet response - of quark and gluon initiated jets, as defined by angular matching to partons in Monte Carlo. This difference is observed to be as high as 8%. Global sequential corrections uses the properties of the jets as well as information from the muon chamber to account for this flavor dependence. The method and results of this correction are discussed in detail in reference [9]

3.5 Residual in-situ calibration

In-situ techniques, employing the balance of physics objects in the transverse plane, are used in the final stage of the JES calibration. The p_T of reference objects (photons, Z bosons or other jets) and the jets being calibrated are compared in both data and Monte Carlo simulation to measure the ratio [8]

$$\langle p_T^{\text{jet}} / p_T^{\text{ref}} \rangle_{\text{data}} = \langle p_T^{\text{jet}} / p_T^{\text{ref}} \rangle_{\text{MC}}$$

This quantity defines a residual correction which is applied to jets reconstructed in data. These in-situ techniques are discussed in detail in references [2] and [8]. These corrections vary from about 1% to 2.5% of the JES (improving with larger p_T). [8]

$\phi = 0$ corresponds to the positive x -axis and increases clockwise looking into the positive z direction. The pseudorapidity η is an approximation for rapidity in the high energy limit, and it is related to the polar angle θ as $\eta = \ln \tan \theta / 2$

4 Random Cones Method for JER

Now, having enumerated the sources of error and procedure to correct the jet energies, we present an analysis of the efficacy of that procedure, i.e. of the jet energy resolution, using the random cones method.

The principle idea of the random cones method is to use "zero bias" events to obtain a measurement of the noise (including noise from pile-up), which contributes to the JER. Zero bias samples are created by recording events exactly one accelerator turn after a high p_T L1 calorimeter trigger. These events will thus be contained in a random filled bunch collision with a rate proportional to the instantaneous luminosity. Next, a cone is projected with a given radius at a random value of η and ϕ . All energy clusters from the zero-bias sample that are found within the random cone are summed up at the constituent scale. This energy is interpreted as the expected value of pile-up fluctuations that would be captured by an anti-kt jet in the same direction. The assumption is justified because cones are a good approximation for the shape of anti-kt jets, based on the way the algorithm is implemented. [11]

To decrease bias, a second cone is projected at $\phi + \pi$ and a new random η . The addition of π to the ϕ value of the second cone helps to ensure that the two cones do not overlap. Due to their non-overlapping nature, the common mode noise fluctuations are expected to be balanced in the two cones. By taking the difference, biases like common mode noise are eliminated.

The JER found for the random cone jets is fitted to a three parameter model (summed in quadrature) as follows:

$$\frac{\sigma(p_T)}{p_T} = \frac{N}{p_T} \oplus \frac{S}{\sqrt{p_T}} \oplus C \quad (1)$$

This functional form is a standard model for calorimeter resolutions. The S term captures uncertainties due to sampling statistics, and is weakly correlated with p_T . The C term reflects the growing uncertainty with growing p_T , largely due to energy leakage outside the active detector regions, and the N term is the so-called noise term. The noise term is independent of p_T and is mainly due to electronic and detector noise, and pile-up. Since pile-up will be the dominant source of fluctuations in our zero-bias events, the random cones method should accurately determine N . [2]

5 Results

5.1 Random Cone Resolution

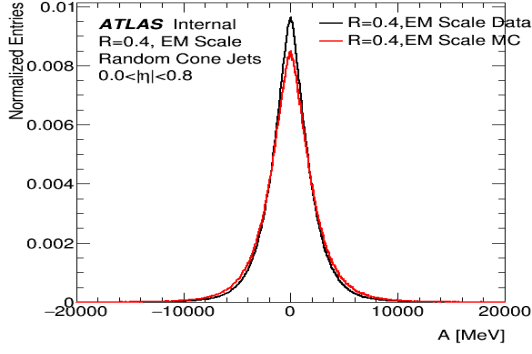
The estimate for the JER using the random cone method, which we will refer to as the RCR (for Random Cone Resolution), is calculated by subtracting the jet p_T in the second cone from that of the first. As explained above, the expected difference is zero, because each cone should contain the same distribution of common mode noise fluctuations from pile-up. Thus, the width of the measured distribution is an estimate of the pile-up contribution to the JER. Plots of this distribution for data and MC are shown in figure 5 (where the difference in random cone p_T is denoted with the variable name A). It is clear that the distributions are centered around 0, as expected. The widths can be seen to be on the order of a few GeV.

The RCR is calculated from the A distributions as follows: First the width of the distribution is obtained. Starting from the mean of the distribution, we move one bin at a time to the right until the area between the center the current bin is greater than 34% of the total area of the histogram. The process is repeated to the left, and the width is defined as the average of difference between these two distances. This width is then divided by $\sqrt{2}$ to give the RCR at the constituent scale.

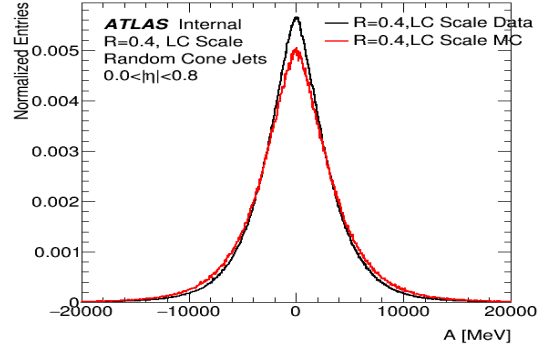
Figure 6 shows RCR vs η and μ across all NPV ranges. We can see that the RCR is roughly constant with respect to η , as expected, and grows linearly with μ . This is also expected, as the RCR is a measure of the contribution to the JER from pile-up noise, and μ is directly correlated to energy from pile-up.

We can also see a weak dependence of the RCR on NPV as well. When there are more primary vertices, we can expect a greater amount of noise. This effect can be seen in figure 7, which shows RCR as a function of μ for two specific values of NPV. This trend holds across different NPV ranges.

Finally, we note that the random cone method is not ideal to analyze noise at high $|\eta|$. At high values of η there is very little energy from pile-up, and thus statistics are very low. After generating a random cone, the random cones algorithm will discard that cone and generate a new one if the energy in that

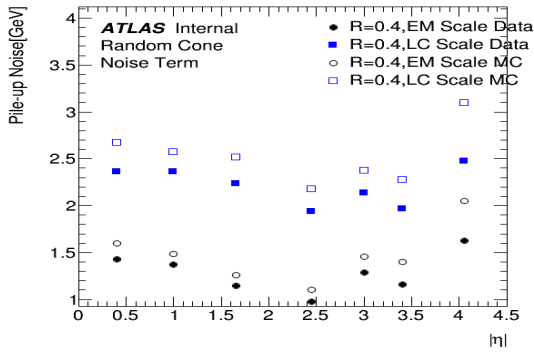


(a) Random cone p_T difference, EM scale

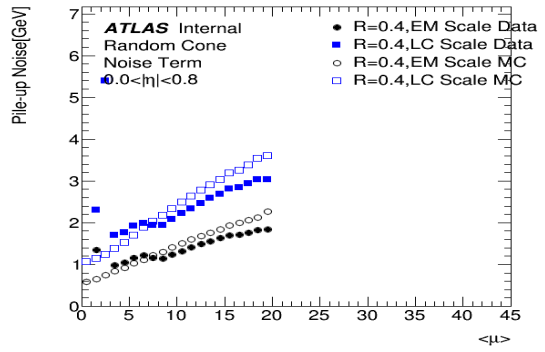


(b) Random cone p_T difference, LC scale

Figure 5: Random cone p_T difference distributions



(a) RCR as a function of η (all NPV)



(b) RCR as a function of μ (all NPV)

Figure 6: Random cone resolution (RCR)

cone did not pass a certain minimum threshold. In our analysis we found that the method begins to skip a large number of cones at high η and thus produces inaccurate estimates of the noise term.

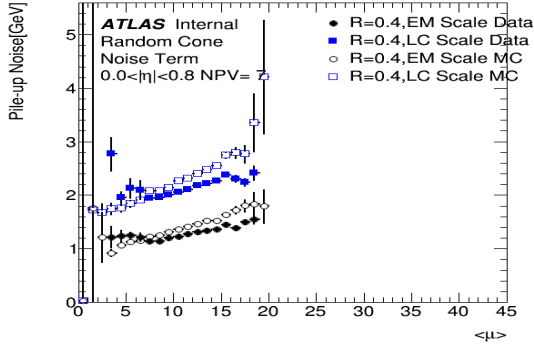
5.2 Error bars

Error bars were generated for the RCR calculations using the following sampling procedure: for each random cone p_T difference distribution, a random number r is generated from a Poisson distribution with mean equal to the number of events in the distribution. A toy is constructed by r events from the distribution. Two-hundred of these toys are made for each random cone distribution. The two-hundred noise terms from the two-hundred toys are then plotted. The mean of these toy distributions is taken as the noise term for that random cone run, and then finally the error is taken to be the RMS of the distribution.

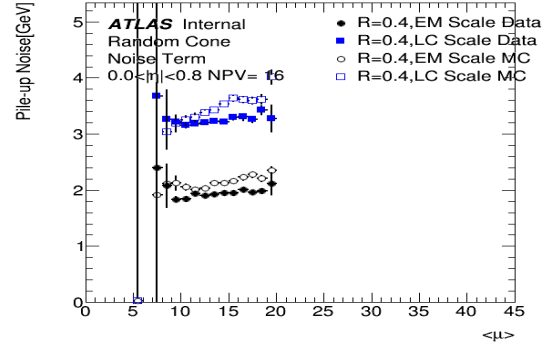
Figure 7 shows the RCR with the error bars generated using the toys. We can see that in general the uncertainty on the RCR is small, except when μ is low. This dependence on μ is expected, because sampling statistics are low when there is not a lot of energy from pile-up.

5.3 Taking RCR to the JES

Now that we have the RCR at the constituent scale, we need to calibrate it to the JES to estimate the noise contribution to the JER. To do this, we define a scale factor $f = p_T^{\text{calib}} / p_T^{\text{PU sub}}$ where $p_T^{\text{PU sub}}$ is the jet p_T after pile-up subtraction at the constituent scale (i.e. before calibration), and the numerator is the total jet p_T at the JES (after the full calibration). The RCR is scaled by the mean of f in each truth jet p_T bin. [10] This process gives results in the curves shown in 8 and 9.



(a) RCR and error bars, NPV = 7



(b) RCR and error bars, NPV = 16

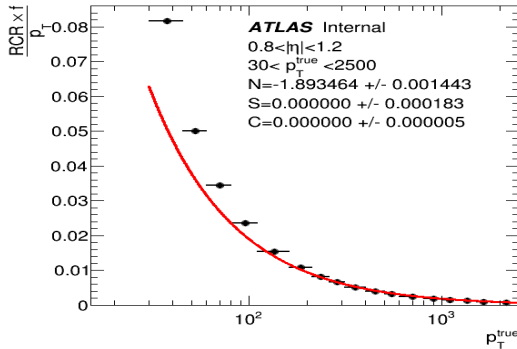
Figure 7: RCR for fixed NPV, with error bars

5.4 Noise Term

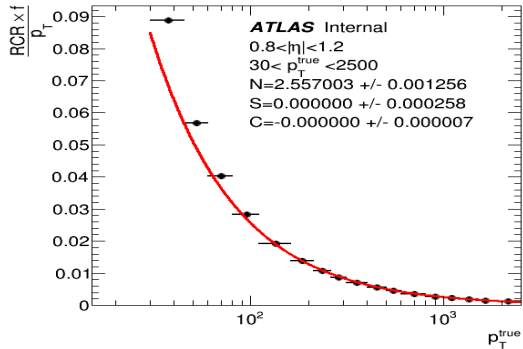
When fitting the RCR distributions to the equation 1 we found an unsatisfactory fit using only the parameters N , C , and S . In order to improve the fit, we found it necessary to modify equation 1. Equation 2 is our improved model.

$$\frac{\sigma(p_T)}{p_T} = \frac{N}{p_T} \oplus \frac{S}{\sqrt{p_T}} \oplus \frac{D}{p_T^{3/2}} \oplus C \quad (2)$$

The terms N , S , and C all retain their significance in this new model. However, we have added an additional term, D , to perform a more accurate fit to the data. RCR with fits to the three parameter equation (1) are shown in figure 8 and our four parameter fit is shown in figure 9. Note that both the fit parameters S and C are effectively zero, which is expected for our zero bias events. The only source of uncertainty from the random cones should be due to noise, N .



(a) EM RCR with fit, $0.8 < |\eta| < 1.2$

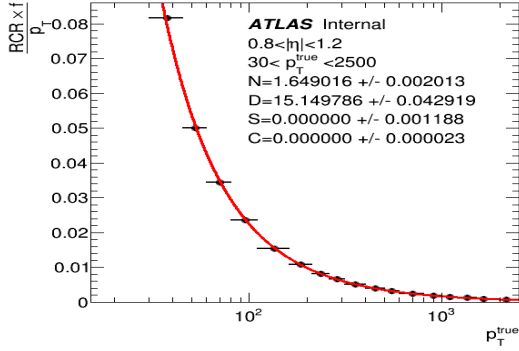


(b) LC RCR with fit, $0.8 < |\eta| < 1.2$

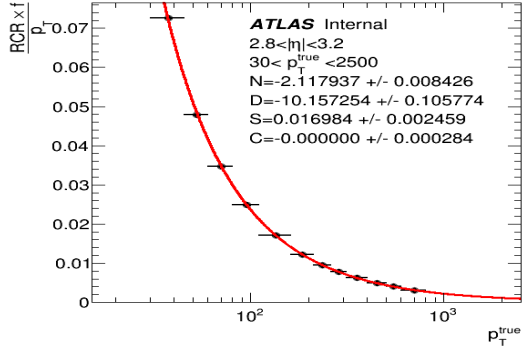
Figure 8: RCR over p_T plots, with fits to three parameter noise model 1. The fits are poor, especially at low p_T .

As a final check on the efficacy of the random cones method, we plot the JER calculated on the MC samples with and without pile-up, their quadratic difference, and the RCR. Figures 10 and 11 show characteristic results of these calculations for two η bins, from EM and LC jets. The red circles show the JER for samples with pile-up, the blue squares show the JER for no pile-up samples, the black triangles are the quadratic difference between the former two measures, and finally the green triangle shows the RCR.

After subtracting in quadrature the no pile-up JER from the pile-up JER, the remaining uncertainties should all be due to pile-up. This curve then, the quadratic difference curve (black triangles), should match the RCR curve (green triangles), since RCR is also a measure of the uncertainty due to pile-up. The ratio of these two curves is plotted in the lower half of each figure. If the curves match as expected,



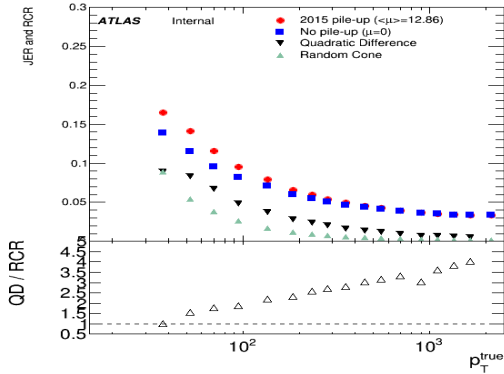
(a) EM RCR over p_T , with fit, $0.8 < |\eta| < 1.2$



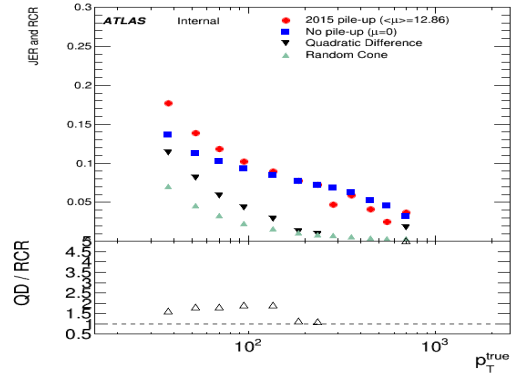
(b) LC RCR over p_T , with fit, $2.8 < |\eta| < 3.2$

Figure 9: Calibrated RCR plots, with fits to four parameter noise model 2. The fits are much stronger with the extra parameter.

then these ratio plots should be equal to unity everywhere. We observe significant deviation from unity, and the effect worsens with increasing p_T .



(a) JER vs RCR, $0.8 < |\eta| < 1.2$



(b) JER vs RCR, $2.8 < |\eta| < 3.2$

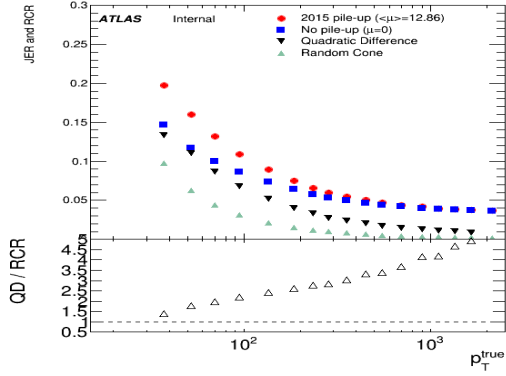
Figure 10: JER and RCR for LC samples

5.5 Closure

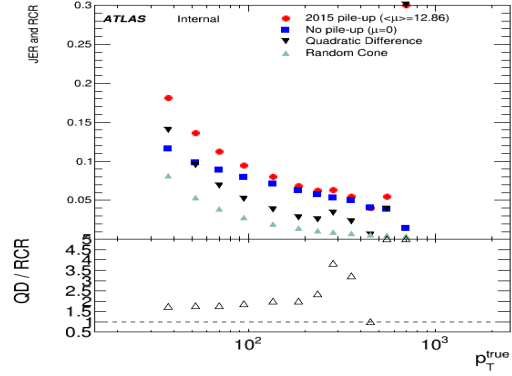
To investigate the discrepancy in the JER calculation versus the RCR calculation, discussed above, we looked at the closure of the JES calibration method. Recall that closure is defined as the ratio of the calibrated p_T to the truth p_T . For a perfect JES calibration, we expect a closure of 1. We find good closure as p_T increases, but poor closure at low p_T . There is also a slight improvement in closure with increasing η . Figures 12 and 13 show the mean $p_T^{\text{calib}}/p_T^{\text{true}}$ for EM and LC samples (i.e. the mean closures from the calibrations), respectively, for two different η bins. Note that closure improves much more rapidly in the samples with pile-up as compared to the samples without pile-up. The non-closure of the JES calibration suggests that something is going wrong with the calibration procedure. We suspect that the error lies within the residual pile-up correction step, because the JES closure differs between the pile-up and no-pile up samples.

6 Conclusions

Our study suggests that the random cone method does not correctly account for of the contribution to the JER from pile-up noise. Figures 10 and 11 clearly show a disagreement between the expected JER and our calculation of the RCR. Our fits of equation 2 to the RCR data are strong, but they do not reveal much about the pile-up noise distribution. The addition of the extra term to the uncertainty model is artificial, a more or less arbitrary mathematical trick to get a good fit. More work needs to be

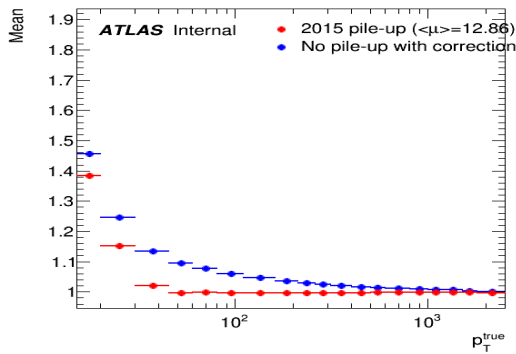


(a) JER vs RCR over p_T , $0.8 < |\eta| < 1.2$

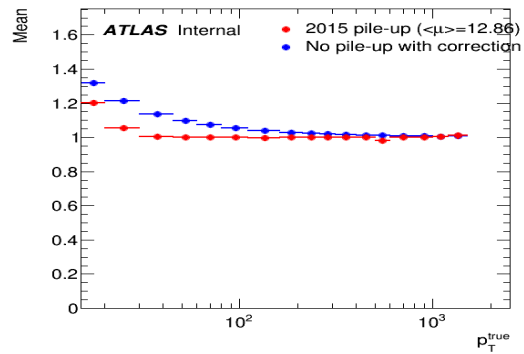


(b) JER vs RCR, $2.8 < |\eta| < 3.2$

Figure 11: JER and RCR for EM samples



(a) $0.8 < |\eta| < 1.2$



(b) $2.8 < |\eta| < 3.2$

Figure 12: Mean JES closure on EM MC samples

done to investigate the non-closure of the JES calibration method before the random cones method can be used effectively to measure the noise term. Once a good calibration is obtained, the noise term can be read off of the fit and used to improve future measurements from the LHC, which will be increasingly important as the beams are operated at higher luminosities.

A Appendix

A.1 Dataset

Our analysis used the zero bias events and the Monte Carlo samples JetM1 and JetM5. Zero bias events are recorded one accelerator turn after a high p_T L1 calorimeter trigger, so that there is an extremely low probability for collisions.

A.2 Process overview

In order to employ and analyze the random cones method, the following steps were performed:

1. Raw data from ATLAS, in the form of DAOD and AOD files from the zero-bias events, was processed into tree objects so that they can be manipulated in ROOT, a data analysis software framework commonly used by ATLAS. More information on ROOT can be found at <https://root.cern.ch>.
2. Random cones were generated, along with 3-D histograms of the random cone jets. These histograms were reweighted according to jet p_T .
3. Different slices of the histograms were plotted using the RandomConeMaker/SavePlots package, and the width of the non-gaussian distributions were calculated.

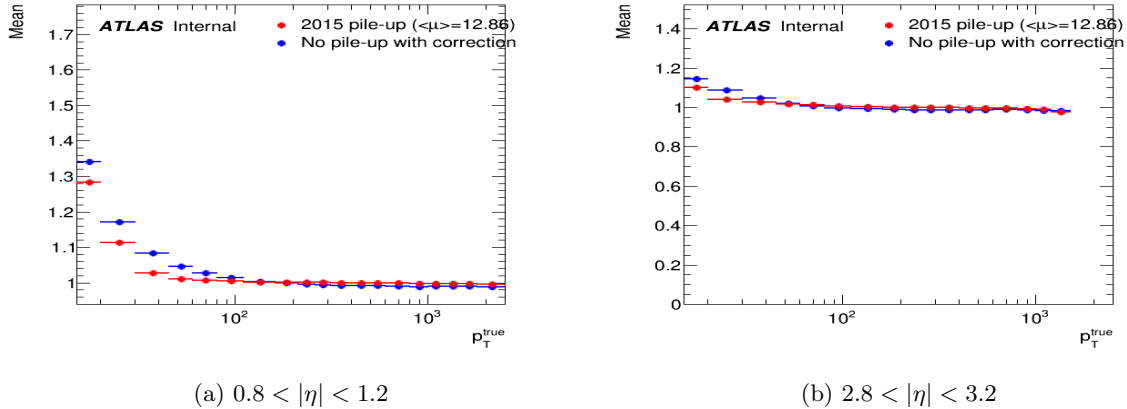


Figure 13: Mean JES closure on LC MC samples

4. Error bars were calculated for the RCR widths using repeated sampling.
5. The ratio of the calibrated jet p_T to the truth jet p_T was plotted for various bins. This ratio should be close to unity for accurate calibrations. These histograms are also reweighted.
6. The model of the JER described in equation 1 was fit to the data; resolution plots were generated and the noise term calculated.
7. The JER was calculated on the MC samples using the width of the $p_T^{\text{calib}}/p_T^{\text{true}}$ distributions.
8. Finally, plots were generated showing the JER in samples with and without pile-up and the difference between the two. This difference was compared to the random cone resolution.

A.3 Source Code

All source code written and used for this study is hosted on GitLab, in four repositories:

1. TreeMaker <https://gitlab.com/khildebrand/TreeMaker>
2. ReweightHistograms <https://gitlab.com/khildebrand/ReweightHistograms>
3. RandomConeMaker <https://gitlab.com/khildebrand/RandomConeMaker>
4. NoiseTermJES <https://gitlab.com/khildebrand/NoiseTermJES>

Acknowledgements

This study would not have been possible without the patient help of Kevin Hildebrand, who also wrote the vast majority of source code used to perform the analysis and create the plots needed. Thanks, Kevin!

References

- [1] The ATLAS collaboration. Atlas jet energy scale. arXiv:1201.2429v1, September 2011.
- [2] The ATLAS collaboration. Jet energy resolution in proton-proton collisions at $s = 7$ tev recorded in 2010 with the atlas detector. arXiv:1210.6210v1, October 2012.
- [3] The ATLAS collaboration. Performance of the atlas trigger system in 2010. *The European Physical Journal C*, 72(1), 2012.
- [4] The ATLAS collaboration. Single hadron response measurement and calorimeter jet energy scale uncertainty with the atlas detector at the lhc. arXiv:1203.1302v1, March 2012.

- [5] The ATLAS collaboration. Jet energy measurement with the atlas detector in proton-proton collisions at $\sqrt{s} = 7$ tev. arXiv:1112.6426, 2013.
- [6] The ATLAS collaboration. Pile-up subtraction and suppression for jets in atlas. ATLAS-CONF-2013-083, August 2013.
- [7] The ATLAS collaboration. Electron reconstruction and identification efficiency measurements with the atlas detector using the 2011 lh proton-proton collision data. arXiv:1404.2240v3, July 2014.
- [8] The ATLAS collaboration. Jet energy scale and its systematic uncertainty in proton-proton collisions at $\sqrt{s} = 7$ tev with atlas 2011 data. ATLAS-CONF-2013-004, January 2014.
- [9] The ATLAS collaboration. Jet global sequential corrections with the atlas detector in proton-proton collisions at $\sqrt{s} = 8$ tev. ATLAS-CONF-2015-002, May 2015.
- [10] The ATLAS collaboration. Monte carlo calibration and combination of in-situ measurements of jet energy scale, jet energy resolution and jet mass in atlas. ATLAS-CONF-2015-037, August 2015.
- [11] Gregory Soyez Matteo Cacciari, Gavin P. Salam. The anti- k_t jet clustering algorithm. arXiv:0802.1189, April 2008.